RSC Advances

PAPER

View Article Online
View Journal | View Issue

Cite this: *RSC Adv.*, 2019, **9**, 33017

Fe^{2+} doped in $CsPbCl_3$ perovskite nanocrystals: impact on the luminescence and magnetic properties†

Yue Hu,[a] Xinyue Zhang,[b] Chaoqun Yang,[a] Ji Li[ab] and Li Wang *[ab]

Received 4th September 2019
Accepted 1st October 2019

DOI: 10.1039/c9ra07069a

rsc.li/rsc-advances

All inorganic halide perovskite nanocrystals (NCs) have wider practical applications owing to their good properties, whereas the photoluminescence quantum yield (PLQY) of the purple emissive $CsPbCl_3$ NCs is too low to apply in multi-color displays. In this study, earth-abundant Fe^{2+} metal ions were successfully incorporated into the lattice of $CsPbCl_3$ NCs with the partial replacement of the sites of Pb^{2+} ions. The impacts of Fe^{2+} ions on the luminescence and magnetic properties of $CsPbCl_3$ NCs were studied using photoluminescence spectroscopy (PL), X-ray diffraction spectroscopy (XRD), transmission electron microscopy (TEM), field emission scanning electron microscopy (FE-SEM), and a vibrating sample magnetometer (VSM). $CsPb_{1-x}Fe_xCl_3$ NCs, with $x = 0$, 0.1, 0.2, and 0.3, were synthesized at 170 °C. It was found that an appropriate amount of Fe^{2+} doping not only improved the homogeneity of the size of NCs, but also enhanced the PLQY and average PL lifetimes. An obvious hysteresis behavior was observed for the NCs, and there was a significant change in the saturation magnetization value with the increase in the Fe^{2+} concentration.

1. Introduction

The outstanding optoelectronic properties of hybrid methylamine lead halide ($MAPbX_3$, $MA = CH_3NH_3^+$; X = Cl, Br, and I), such as a direct optical band gap, large optical absorption coefficient, long-range diffusion length, and high charge carrier mobility, have made their rapid development for application in photovoltaic devices with an enormous potential in solar cells, lasers, and photodetectors.[1–4] However, they are extremely sensitive to oxygen and moisture, which severely limit their further development and practical applications.[5,6] In 1990s, all inorganic $CsPbX_3$ (X = Cl, Br, and I) nanocrystals (NCs) appeared.[7–9] They have good environmental stability, a high photoluminescence quantum yield (PLQY), a narrow emission linewidth, and a wide color gamut compared to hybrid methylamine lead halide, which led to their quick practical applications.[10,11]

In the practical applications of lead perovskite halides, the biggest problem is the environment pollution caused by the toxicity of lead. The most effective way is to replace Pb ions in the crystal structure by introducing impurity ions. Recently, some researchers reported the transition and alkaline earth metal ion doping into perovskite NCs.[12–15] For example, Belcher *et al.* demonstrated for the first time that partially substituting Pb^{2+} by Co^{2+} at the B-sites of the perovskite lattice was possible.[16] Sun *et al.* had shown that the doping of $CsPbX_3$ NCs with Ni^{2+} ions enabled single-color violet luminescence with near-unity PLQYs.[17] Among these ions, being the most abundant element on earth, Fe ions are not only environmentally friendly and low-cost, but also have a good conductivity. Moreover, Strouse *et al.* proved the appearance of room-temperature ferromagnetism in Fe-doped CdSe nanoparticles.[18] Therefore, replacing Pb ions in lead perovskite halides with Fe ions has become a popular direction for their application as photonic devices. The structural, electronic, magnetic and optical properties of the perovskite CH_3NH_3(-Pb:Fe)I_3 were systematically studied from first principles and experiments by Hao *et al.*[19]. Also, Yu *et al.*[20] doped different concentration of Fe^{2+}/Fe^{3+} into the crystal lattice of $MAPbCl_3$ single crystals, and studied the crystal growth process, crystal structure, optical and optoelectronic properties.

In all inorganic lead perovskite materials, the PLQYs of green and red emissive $CsPbBr_3$ and $CsPbI_3$ NCs have reached 90%, respectively,[21,22] whereas the PLQY of purple emissive $CsPbCl_3$ NCs is still low (below 5%).[23] Therefore, the most urgent task now is to enhance the PLQY of $CsPbCl_3$ NCs for the application of violet-emitting devices. Song *et al.* enhanced the exciton emission QY of $CsPbCl_3$ NCs up to 10.3% and 31.2% by doping K and Eu ions, respectively.[24] Singh *et al.* synthesized Fe^{3+}-

[a]Key Laboratory of Functional Materials Physics and Chemistry of the Ministry of Education, Jilin Normal University, Siping 136000, China. E-mail: wangli@jlnu.edu.cn

[b]National Demonstration Center for Experimental Physics Education, Jilin Normal University, Siping 136000, China

† Electronic supplementary information (ESI) available. See DOI: 10.1039/c9ra07069a

doped $CsPbCl_3$ NCs and found that the doping of Fe enhanced the PL QY from 1.85 to 4.32.[25]

In this study, we synthesized and researched $CsPb_{1-x}Fe_xCl_3$ (x = 0, 0.1, 0.2, and 0.3) NCs. Interesting changes in luminescence and magnetic properties were observed by varying the doping concentration of Fe^{2+} ions in $CsPbCl_3$ NCs. The samples were characterized *via* various techniques and are discussed in detail.

2. Experimental

2.1 Materials

Lead chloride ($PbCl_2$, 99.99%), cesium carbonate (Cs_2CO_3, 99.99%), iron dichloride ($FeCl_2$, 99.99%) and trioctylphosphine (TOP, 90%) were purchased from Aladdin; 1-octadecene (ODE, 90%) was purchased from Alfa Aesar; oleic acid (OA, 90%) and oleylamine (OLA, 70%) were purchased from Aldrich. All chemicals were used without further purification.

2.2 Synthesis of $CsPb_{1-x}Fe_xCl_3$ (x = 0, 0.1, 0.2, and 0.3) NCs

Cs-oleate precursors and $CsPbCl_3$ NCs were synthesized following our previous reports.[26,27] In a typical procedure for the synthesis of Fe^{2+} doped $CsPbCl_3$ NCs, $PbCl_2$ ($1-x$ mmol) and $FeCl_2$ (x mmol) were mixed with OLA (1.5 mL), OA (1.5 mL), TOP (1 mL), and ODE (10 mL) in a 50 mL three-neck round-bottomed flask. The reaction mixture was degassed at 110 °C for 20 min, and then heated up to 170 °C under an argon flow. A Cs-oleate precursor (1 mL) was quickly injected and 15 s later, the reaction mixture was cooled using an ice-water bath. The solution was centrifuged for 5 min at 5000 rpm after the reaction, the supernatant was discarded and then, the particles were dispersed in hexane and centrifuged again for 5 min at 5000 rpm to remove the residual reaction mixture.

2.3 Characterization

X-ray diffraction (XRD) was performed by incident radiation from a Rigaku D/Max-2500 diffractometer and copper Kα radiation (λ = 1.54 A). UV-visible absorption spectra were recorded using a Shimadzu UV-2700 spectrophotometer. The steady-state and time-resolved fluorescence spectra were collected using a Horiba Jobin Yvon fluorologo-3 fluorescence spectrometer; a 450 W Xenon lamp and an N-305 nano-LED were used as the excitation sources. The absolute photoluminescence quantum yield (PLQY) was recorded using an Otsuka QE-2000. Transmission electron microscopy (TEM) was performed using a JEOL-JEM-2100 microscope. Field emission scanning electron microscopy (FE-SEM) and energy-dispersive X-ray (EDX) mapping were performed using a JEOL JSE-7800F. A vibrating sample magnetometer (VSM, Lake Shore 7407) was used to determine the magnetic properties.

3. Results and discussion

Fig. 1(a) shows the XRD patterns of $CsPb_{1-x}Fe_xCl_3$ NCs. For undoped $CsPbCl_3$ NCs, there are two strong diffraction peaks around 15.4° and 31.6°, corresponding to the (100) and (200) planes. It indicates that the typical cubic structure has been formed, fitting with the reference from a standard card (JCPDS: 75-0411). With different concentrations of Fe^{2+} ion doping, no new diffraction peaks appeared, which insinuates that the structure of NCs is maintained even after the doping with Fe^{2+} ions. The enlarged patterns of (200) the diffraction peaks for the samples are shown in Fig. 1(b). With the increase in x value, the diffraction peak shifts to a larger angle. It suggests that Fe^{2+} ions have been doped into $CsPbCl_3$ NCs, and the lattice parameter decreases with the increase in the x value. The decrease in the lattice parameter is due to the fact that the radius of Pb^{2+} (0.120 nm) ions is larger than that of Fe^{2+} (0.076 nm) ions, which is similar to the Ni and Mn ion doped $CsPbCl_3$ NCs.[28]

The TEM images of undoped $CsPbCl_3$ NCs and Fe-doped $CsPbCl_3$ NCs with different doping concentrations are shown in Fig. 2. The inset denotes the particle size distribution. It can be clearly seen that the NCs are monodispersed cubes. Undoped NCs as large as 8.0 nm are distributed between 5.5 and 13.5 nm. After the doping of Fe^{2+} ions, the average sizes and the distribution of the NCs have changed. For x = 0.1, 0.2, and 0.3, the average sizes of the NCs are 6.7, 7.8 and 7.4 nm, and they are distributed in the ranges of 5–10.5 nm, 6.5–10.5 nm, and 4.5–

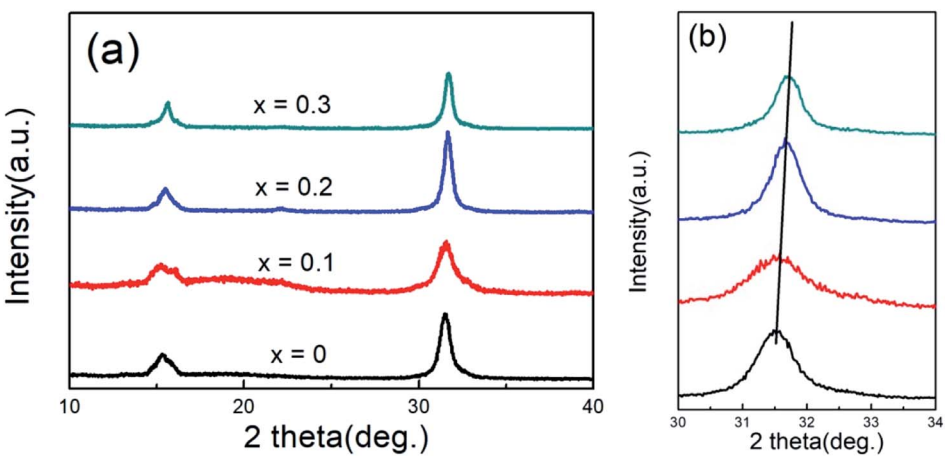

Fig. 1 (a) XRD patterns of $CsPb_{1-x}Fe_xCl_3$ (x = 0, 0.1, 0.2, and 0.3) NCs. (b) The enlarged XRD patterns near 31.6°.

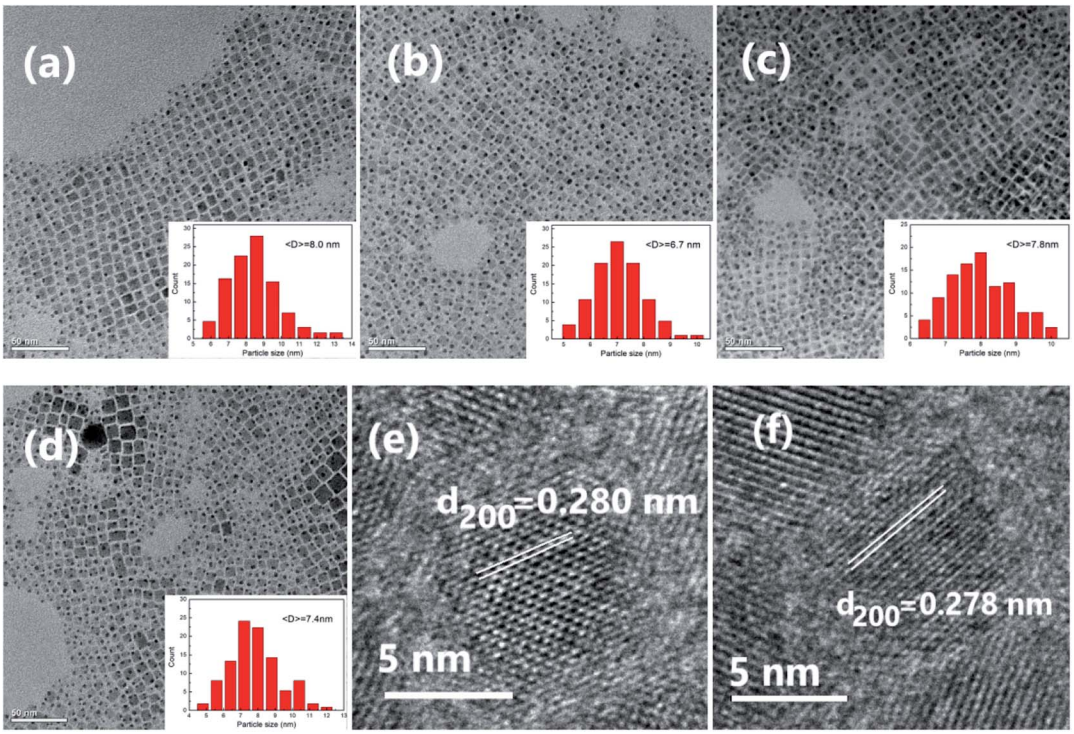

Fig. 2 TEM images of undoped $CsPbCl_3$ NCs (a) and Fe-doped $CsPbCl_3$ NCs with different doping concentrations: (b) $x = 0.1$, (c) $x = 0.2$, and (d) $x = 0.3$. The inset denotes the particle size distribution. The HR-TEM images of undoped $CsPbCl_3$ NCs (e) and Fe-doped $CsPbCl_3$ NCs with $x = 0.1$ (f).

12.5 nm, respectively. The sizes of Fe^{2+}-doped NCs are smaller than those of the undoped NCs, which may be due to the reduction in the growth rate of perovskite NCs in the presence of Fe chloride in the reaction process. Moreover, the size distributions of the NCs with low doping concentrations ($x = 0.1$ and 0.2) are relatively uniform. The high resolution transmission electron microscopy (HR-TEM) images of the undoped $CsPbCl_3$ NCs and Fe-doped $CsPbCl_3$ NCs with $x = 0.1$ are shown in Fig. 2(e) and (f), respectively. The lattice spacing of NCs in the (200) direction is estimated to be about 0.278 nm for Fe^{2+}-doped $CsPbCl_3$ NCs, which is smaller than that for the undoped $CsPbCl_3$ NCs (0.281 nm). The result is consistent with that of XRD analysis and previous reports.[24] In addition, EDX mapping images in Fig. S1† further prove that the elements of Cs, Pb, Cl and Fe are identified in Fe-doped $CsPbCl_3$ NCs.

Fig. 3(a) and (b) show the UV-visible absorption and steady-state PL spectra of $CsPb_{1-x}Fe_xCl_3$ NCs. In Fig. 3(a), the exciton absorption band of undoped $CsPbCl_3$ NCs is about 397 nm. With the increase in the x value, the exciton absorption band monotonously decreases slightly. According to the absorption spectra, the band gaps of the NCs with $x = 0$, 0.1, 0.2, and 0.3 are 3.12, 3.15, 3.16, and 3.18 eV, respectively. The gradual increase in the band gap of the NCs is due to the lattice contraction with the doping of Fe^{2+}. Moreover, in Fig. 3(b), the exciton PL peak is at 404 nm with a full width at half maximum (FWHM) of 15.7 nm (121.0 meV) for undoped $CsPbCl_3$ NCs. For the doped NCs with $x = 0.1$, 0.2 and 0.3, the exciton PL peaks are located at 401, 403 and 402 nm with the FWHM of 13.9 nm (101.8 meV), 13.8 nm (99.1 meV) and 14.6 nm (123.6 meV), respectively. The shift in the PL bands can be caused by the change in the size of NCs, which is corresponding to the quantum size effect of $CsPbX_3$ NCs.[29] With the decrease in the size of NCs, PL bands will have a blue-shift. Moreover, PL bands will have a red-shift when the size increases. The variation in the FWHM of the PL band in the doped NCs may be due to the size distribution of NCs. The distributions of the NCs with low doping levels ($x = 0.1$ and 0.2) are relatively homogeneous, resulting in a small FWHM. The PLQY of $CsPb_{1-x}Fe_xCl_3$ NCs is recorded in Fig. 3(c). The PLQY is 4.4% for the undoped $CsPbCl_3$ NCs, which is slightly higher than that of previous reports,[24,25] but is still below 5%. With the doping of Fe^{2+} ions, the PLQY increases initially, reaching a maximum as x is 0.2, and then decreases with the further increase in the Fe^{2+} ion doping concentration. The maximum PLQY of doped NCs is about 6.2%, which enhanced 1.4 times compared to that of undoped $CsPbCl_3$ NCs. It can be the reduction of defects in Fe^{2+}-doped $CsPbBr_3$ NCs, which leads to the more ordered local environment and the homogeneous distribution of the NCs.[30]

The PL decay curves of undoped $CsPbCl_3$ NCs and Fe doped $CsPbBr_3$ NCs as a function of Fe^{2+} doping concentration are shown in Fig. 3(d). The lifetimes were acquired by fitting the decay curves *via* the function:

$$I(t) = A_1 \exp(-t/\tau_1) + A_2 \exp(-t/\tau_2) \quad (1)$$

The average PL lifetimes were calculated by the following formula:

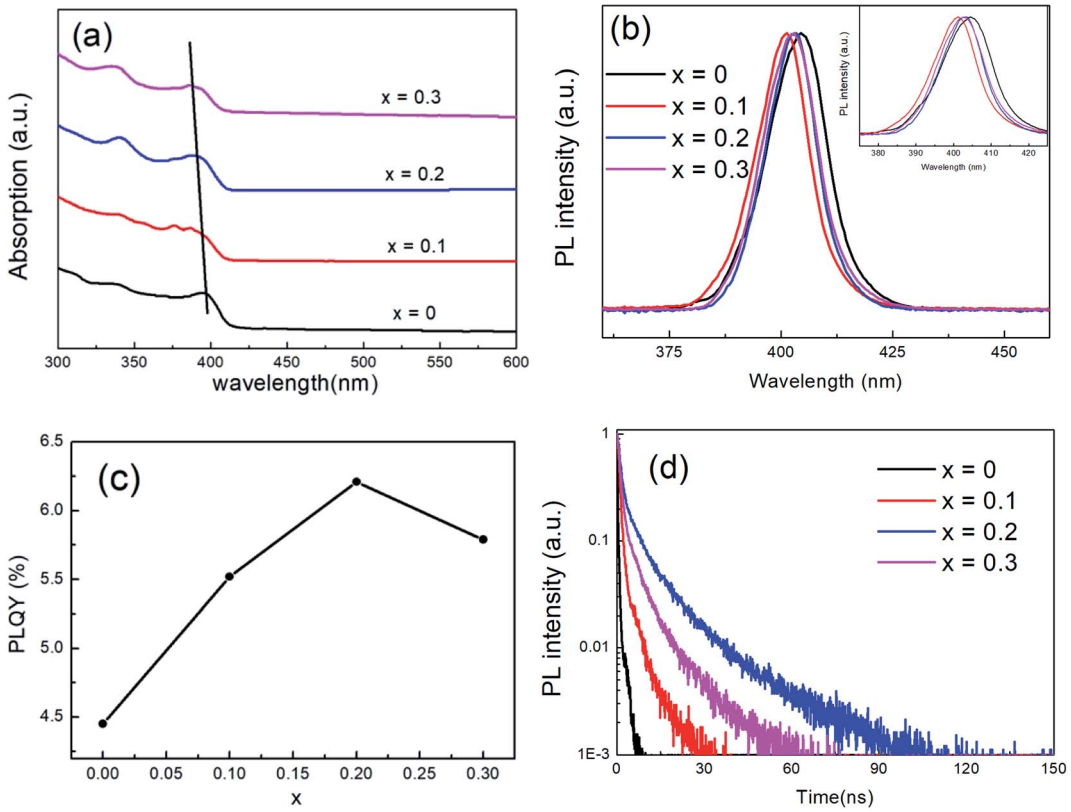

Fig. 3 Absorption (a) and PL spectra (b), PLQYs (c) and decay (d) of $CsPb_{1-x}Fe_xCl_3$ NCs. Inset of (b) shows the enlarged spectra.

$$\tau_{av} = (A_1\tau_1^2) + (A_2\tau_2^2)/(A_1\tau_1) + (A_2\tau_2) \quad (2)$$

where the short-lived process (τ_1) is associated with the energy transfer to trap states, and the long-lived component (τ_2) is related to the exciton recombination transitions.[31] Table 1 lists the fitting results. The values of τ_1, τ_2, and τ_{av} firstly increase, and then decrease with the increase in the Fe^{2+} doping, which is in accordance with the change of PLQY. The maximum of the average PL lifetimes is about 14.6 ns when x is 0.2, which is larger than that of $Cs_xK_{1-x}PbCl_3$ (13.6 ns) and $CsPbCl_3$:Rb (10.2 ns) quantum dots.[24,32]

The contributions of short time and longtime components to the average lifetime are shown in Fig. 4. It is obvious that the contribution of short time components is larger than that of long time components for all the samples, which indicates that the short-lived process dominates in the PL process of $CsPb_{1-x}Fe_xCl_3$ NCs and there are lots of defects in the NCs. Simultaneously, the increase in τ_1 is the indirect evidence that the defect states of Fe-doped $CsPbBr_3$ NCs are reduced and the non-radiative paths are partly eliminated with the doping of Fe^{2+}. It is the main reason for the improvement in the PLQYs of Fe-doped $CsPbBr_3$ NCs, compared to the undoped one. In addition, τ_1 of $CsPb_{0.7}Fe_{0.3}Cl_3$ NCs is less than that of $CsPb_{0.8}Fe_{0.2}Cl_3$ NCs, demonstrating that the former have more defects than the latter. Therefore, the excessive doping of Fe^{2+} ions may destroy the lattice structure of $CsPbBr_3$ NCs, resulting in a decrease in PLQY and average PL lifetimes.

The PL spectra of $CsPb_{0.8}Fe_{0.2}Cl_3$ NCs were recorded at temperatures ranging from 80 K to 300 K, as shown in Fig. 5(a). The asymmetry of the PL spectrum for the NC at 80 K is caused

Table 1 PL lifetimes of $CsPb_{1-x}Fe_xCl_3$ NCs

	A_1	τ_1 (ns)	A_2	τ_2 (ns)	τ_{av} (ns)
0	1.069	0.6	0.005	5.9	0.8
0.1	1.097	0.9	0.020	11.2	2.8
0.2	0.869	2.6	0.215	20.8	14.6
0.3	0.985	2.4	0.118	16.8	9.0
Error	±0.004	±0.4	±0.003	±0.3	±0.3

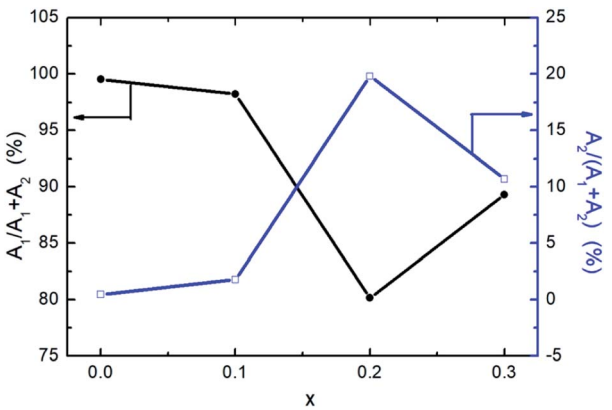

Fig. 4 Contributions of short time components (A_1) and long time components (A_2) of $CsPb_{1-x}Fe_xCl_3$ NCs.

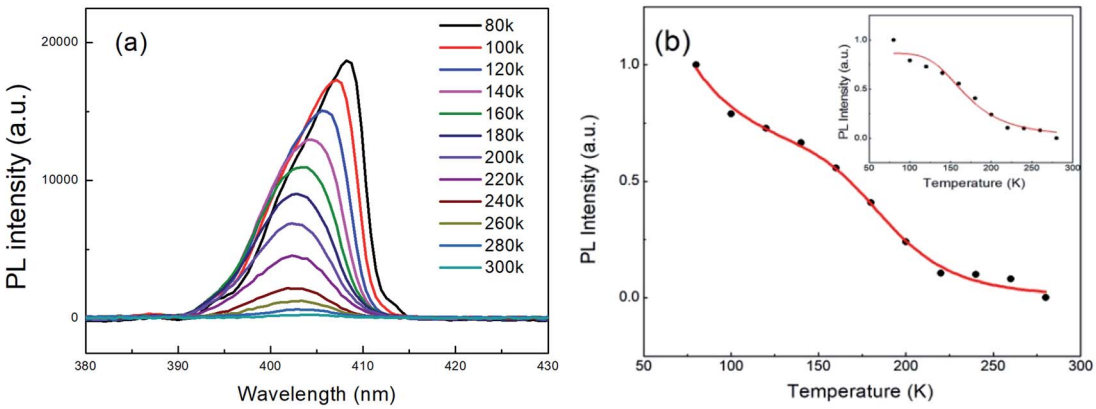

Fig. 5 (a) The PL spectra of $CsPb_{0.8}Fe_{0.2}Cl_3$ NCs at various temperatures. (b) Variation of integrated PL intensity with respect to temperature.

by the size distribution.[33] As the temperature increases from 80 K to 300 K, it shows a clear decrease in the PL intensity accompanied by a broadening in the emission bandwidth. The decrease in the PL intensity is related to the increase in the FWHM of the PL peak, which can be attributed to the phonon-assisted broadening effect. A similar case was also observed in CdSe quantum dots.[34,35] It is worth noting that there is a blue-shift in the emission energy when the temperature increases from 80 K to 200 K, then has a small redshift with the further increase in temperature. The blue-shift with the increase in temperature is due to the fact that the out-of-phase band-edge states suffer from lattice dilation at the Brillouin zone boundary.[36] Also, the red-shift above 200 K may be attributed to the defect states in the NCs. Fig. 5(b) gives the Arrhenius plot of the integrated PL intensity *versus* temperature, fitted using the equation below:[37]

$$I(T) = \frac{I_0}{1 + C_1 \exp\left(-\frac{E_{a1}}{k_B T}\right) + C_2 \exp\left(-\frac{E_{a2}}{k_B T}\right)} \quad (3)$$

where I_0 is the initial intensity; the constants C_1 and C_2 are the densities of nonradiative recombination centers with activation energies E_{a1} and E_{a2}, respectively. By fitting Fig. 5(b) to eqn (3), two activation energies, $E_{a1} \approx 168 \pm 25$ meV ($C_1 \approx 1.1 \times 10^6$) and $E_{a2} \approx 7 \pm 2$ meV ($C_2 \approx 71.8$) were obtained. The majority of the contribution is coming from E_{a1} because C_1 is larger than C_2, but two activation energies caused by the distribution of different energy nonradiative centers is observed here. A similar result was reported for $CsPbBr_3$ NCs.[38] It is worth noting when a single activation energy ($E_a \approx 96 \pm 18$ meV) is considered, the integrated PL intensity *versus* temperature is a poor fit (seeing illustration in Fig. 5(b)).

Fig. 6 shows the magnetic hysteresis loops measured at room temperature. An obvious hysteresis behavior has been observed for the samples. For undoped $CsPbCl_3$ NCs, the saturation magnetization M_s is only 0.13 meum g^{-1} at room temperature. Upon increasing the concentration of Fe^{2+} ions, an increase in M_s was observed. The observed ferromagnetism of doped NCs may be attributed to the presence of Fe^{2+} ions in the lattice as a substituent for carrier-induced ferromagnetism.[39]

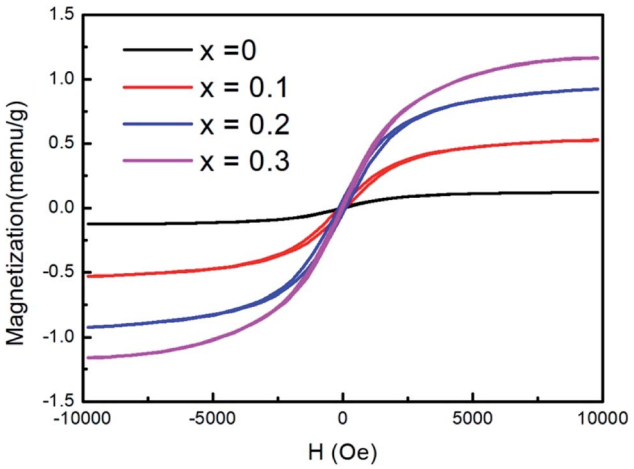

Fig. 6 Hysteresis loops of $CsPb_{1-x}Fe_xCl_3$ NCs at room temperature.

4. Conclusions

In summary, we have studied the luminescent and magnetic properties of $CsPb_{1-x}Fe_xCl_3$ NCs with $x = 0$, 0.1, 0.2, and 0.3. The diffraction peaks in XRD patterns shifted toward a larger angle, indicating the successful doping of Fe into $CsPbCl_3$ NCs. The TEM images show that the size distributions of $CsPb_{1-x}Fe_xCl_3$ NCs with $x = 0.1$ and 0.2 were relatively uniform. After an appropriate amount of Fe^{2+} doping ($x = 0.2$), the PLQY of excitons is enhanced from 4.4% to 6.2%, and the average PL lifetimes is lengthened from 0.91 ns to 14.61 ns. While the excessive doping will destroy the lattice structure of the perovskite NCs, resulting in the decrease in the PLQY and average PL lifetimes. The increase in PLQY suggests that the defect states and the non-radiative paths of the NCs decrease with doping Fe^{2+} ions. Beside that there is a significant change in the saturation magnetization value with the increase in the Fe^{2+} ion concentration, and the ferromagnetism of doped NCs may be attributed to the presence of Fe^{2+} ions in the lattice as a substituent for carrier-induced ferromagnetism.

Conflicts of interest

There are no conflicts to declare.

Acknowledgements

This work was supported by the National Natural Science Foundation of China (11504132) and the Thirteenth Five-Year Program for Science and Technology of Education Department of Jilin Province (JJKH20180768KJ).

References

1 J. H. Im, I. H. Jang, N. Pellet, M. Grätzel and N. G. Park, *Nat. Nanotechnol.*, 2014, **9**, 927–932.
2 F. X. Xie, D. Zhang, H. Su, X. Ren, K. S. Wong, M. Grätzel and W. C. Choy, *ACS Nano*, 2015, **27**, 639–946.
3 F. Fu, L. Kranz, S. Yoon, J. Löckinger, T. Jäger, J. Perrenoud, T. Feurer, C. Gretener, S. Buecheler and A. N. Tiwari, *Phys. Status Solidi A*, 2015, **212**, 2708–2717.
4 D. Liu, L. Wu, C. Li, S. Ren, J. Zhang, W. Li and L. Feng, *ACS Appl. Mater. Interfaces*, 2015, **7**, 16330–16337.
5 A. Dualeh, N. Tétreault, T. Moehl, P. Gao, M. K. Nazeeruddin and M. Grätzel, *Adv. Funct. Mater.*, 2014, **24**, 3250–3258.
6 J. Su, D. P. Chen and C. T. Lin, *J. Cryst. Growth*, 2015, **422**, 75–79.
7 L. Protesescu, S. Yakunin, M. I. Bodnarchuk, F. Krieg, R. Caputo, C. H. Hendon, R. X. Yang, A. Walsh and M. V. Kovalenko, *Nano Lett.*, 2015, **15**, 3692–3696.
8 M. A. Uddin, J. K. Mobley, A. A. Masud, T. Liu, R. L. Calabro, D. Y. Kim, C. I. Richards and K. R. Graham, *J. Phys. Chem. C*, 2019, **123**, 18103–18112.
9 S. Seth, T. Ahmed, A. De and A. Samanta, *ACS Energy Lett.*, 2019, **4**, 1610–1618.
10 P. Liang, P. Zhang, A. Pan, K. Yan, Y. S. Zhu, M. Y. Yang and L. He, *ACS Appl. Mater. Interfaces*, 2019, **11**, 22786–22793.
11 J. H. Cha, K. Noh, W. Yin, Y. Lee, Y. Park, T. K. Ahn, A. Mayoral, J. Kim, D. Y. Jung and O. Terasaki, *J. Phys. Chem. Lett.*, 2019, **10**, 2270–2277.
12 S. D. Adhikari, R. K. Behera, S. Bera, N. Pradhan and J. Phys, *Chem. Lett.*, 2019, **10**, 1530–1536.
13 J. K. Chen, J. P. Ma, S. Q. Guo, Y. M. Chen, Q. Zhao, B. B. Zhang, Z. Y. Li, Y. Zhou, J. S. Hou, Y. Kuroiwa, C. Moriyoshi, O. M. Bakr, J. Y. Zhang and H. T. Sun, *Chem. Mater.*, 2019, **31**, 3974–3983.
14 W. Z. Xu, L. Y. Zheng, X. T. Zhang, Y. Cao, T. Y. Meng, D. Z. Wu, L. Liu, W. P. Hu and X. Gong, *Adv. Energy Mater.*, 2018, **8**, 1703178.
15 H. Shao, X. Bai, H. Cui, G. Pan, P. Jing, S. Qu, J. Zhu, Y. Zhai, B. Dong and H. Song, *Nanoscale*, 2018, **10**, 1023–1029.
16 M. T. Klug, A. Osherov, A. A. Haghighirad, S. D. Stranks, P. R. Brown, S. Bai, J. T. W. Wang, X. N. Dang, V. Bulovic, H. J. Snaith and A. M. Belcher, *Energy Environ. Sci.*, 2017, **10**, 236–246.
17 Z. J. Yong, S. Q. Guo, J. P. Ma, J. Y. Zhang, Z. Y. Li, Y. M. Chen, B. B. Zhang, Y. Zhou, J. Shu, J. L. Gu, L. R. Zheng, O. M. Bakr and H. T. Sun, *J. Am. Chem. Soc.*, 2018, **140**, 9942–9951.
18 S. B. Singh, M. V. Limaye, S. K. Date, S. Gokhale and S. K. Kulkarni, *Phys. Rev. B*, 2009, **80**, 235421.
19 L. Zhou, J. J. Chang, Z. H. Lin, C. F. Zhang, D. Z. Chen, J. C. Zhang and Y. Hao, *RSC Adv.*, 2017, **7**, 54586–54593.
20 X. H. Cheng, L. Jing, Y. Yuan, S. J. Du, J. Zhang, X. Y. Zhan, J. X. Ding, H. Yu and G. D. Shi, *J. Phys. Chem. C*, 2019, **123**, 1669–1676.
21 Z. K. Tan, R. S. Moghaddam, M. L. Lai, P. Docampo, R. Higler, F. Deschler, M. Price, A. Sadhanala, L. M. Pazos, D. Credgington, F. Hanusch, T. Bein, H. J. Snaith and R. H. Friend, *Nat. Nanotechnol.*, 2014, **9**, 687–692.
22 F. Liu, Y. H. Zhang, C. Ding, S. Kobayashi, T. Izuishi, N. Nakazawa, T. Toyoda, T. Ohta, S. Hayase, T. Minemoto, K. Yoshino, S. Y. Dai and Q. Shen, *ACS Nano*, 2017, **11**, 10373–10383.
23 H. W. Liu, Z. N. Wu, J. R. Shao, D. Yan, H. Gao, Y. Liu, W. L. Yu, H. Zhang and B. Yang, *ACS Nano*, 2017, **11**, 2239–2247.
24 P. J. S. Rana, T. Swetha, H. Mandal, A. Saeki, P. R. Bangal and S. P. Singh, *J. Phys. Chem. C*, 2019, **123**, 17026–17034.
25 Y. A. Liu, G. C. Pan, R. Wang, H. Shao, H. Wang, W. Xu, H. N. Cui and H. W. Song, *Nanoscale*, 2018, **10**, 14067–14072.
26 L. L. Fei, X. Yuan, J. Hua, M. Ikezawa, R. S. Zeng, H. B. Li, Y. Masumoto and J. L. Zhao, *Nanoscale*, 2018, **10**, 19435–19442.
27 Q. Y. Li, S. H. Ji, X. Yuan, J. Li, Y. Fan, J. H. Zhang, J. L. Zhao and H. B. Li, *J. Phys. Chem. C*, 2019, **123**, 14849–14857.
28 K. Xing, X. Yuan, Y. Wang, J. Li, Y. Wang, Y. Fan, L. Yuan, K. Li, Z. Wu, H. Li, J. Zhao and J. Zhao, *J. Phys. Chem. Lett.*, 2019, **10**, 4177–4184.
29 M. A. Becker, R. Vaxenburg, G. Nedelcu, P. C. Sercel, A. Shabaev, M. J. Mehl, J. G. Michopoulos, S. G. Lambrakos, N. Bernstein, J. L. Lyons, T. Stoferle, R. F. Mahrt, M. V. Kovalenko, D. J. Norris, G. Raino and A. L. Efros, *Nature*, 2018, **553**, 189–193.
30 Z. F. Tan, J. H. Li, C. Zhang, Z. Li, Q. S. Hu, Z. W. Xiao, T. Kamiya, H. Hosono, G. D. Niu, E. Lifshitz, Y. B. Cheng and J. Tang, *Adv. Funct. Mater.*, 2018, **28**, 1801131.
31 G. Pan, X. Bai, D. W. Yang, X. Chen, P. T. Jing, S. N. Qu, L. J. Zhang, D. L. Zhou, J. Y. Zhu, W. Xu, B. Dong and H. W. Song, *Nano Lett.*, 2017, **17**, 8005–8011.
32 Z. Y. Zhao, W. Xu, G. C. Pan, Y. A. Liu, M. Yang, S. W. Hua, X. Chen, H. S. Peng and H. W. Song, *Mater. Res. Bull.*, 2019, **112**, 142–146.
33 M. Koolyk, D. Amgar, S. Aharon and L. Etgar, *Nanoscale*, 2016, **8**, 6403–6409.
34 Y. Zhao, C. Riemersma, F. Pietra, R. Koole, C. M. Donega and A. Meijerink, *ACS Nano*, 2012, **6**, 9058–9067.
35 C. Bullen and P. Mulvaney, *Langmuir*, 2006, **22**, 3007–3013.
36 A. D. Wright, C. Verdi, R. L. Milot, G. E. Eperon, M. A. Perez-Osorio, H. J. Snaith, F. Giustino, M. B. Johnston and L. M. Herz, *Nat. Commun.*, 2016, **7**, 11755.
37 D. Bimberg, M. Sondergeld and E. Grobe, *Phys. Rev. B*, 1971, **4**, 3451.
38 A. Dey, P. Rathod and D. Kabra, *Adv. Opt. Mater.*, 2018, **6**, 1800109.
39 J. K. Bindra, G. Kurian, J. H. Christian, J. V. Tol, K. Singh, N. S. Dalal, M. D. Mochena, S. A. Stoian and G. F. Strouse, *Chem. Mater.*, 2018, **30**, 8446–8456.

